Poly(L-lactide)/Polypropylene Blends: Evaluation of Mechanical, Thermal, and Morphological Characteristics

Priyanka Choudhary, Smita Mohanty, Sanjay K. Nayak, Lakshmi Unnikrishnan

Laboratory for Advanced Research in Polymeric Materials, Central Institute of Plastics Engineering and Technology, Bhubaneswar 751 024, India

Received 5 May 2010; accepted 29 November 2010
DOI 10.1002/app.33866
Published online 11 April 2011 in Wiley Online Library (wileyonlinelibrary.com).

ABSTRACT: Poly(Llactide) (PLA) was blended with polypropylene (PP) at various ratios (PLA:PP = 90 : 10, 80 : 20, 70 : 30, and 50 : 50) with a melt-blending technique in an attempt to improve the melt processability of PLA. Maleic anhydride (MAH)-grafted PP and glycidyl methacrylate were used as the reactive compatibilizers to induce miscibility in the blend. The PLA/PP blend at a blend ratio of 90 : 10, exhibited optimum mechanical performance. Differential scanning calorimetry and thermogravimetric analysis studies showed that the PLA/PP/MAH-*g*-PP blend had the maximum thermal stability with the support of the heat deflection temperature values. Furthermore, dynamic mechanical analysis findings revealed an increase in the glass-transition temperature and storage modulus with the addition of MAH-*g*-PP compatibilizer. The interaction between the compatibilizers and constituent polymers was confirmed from Fourier transform infrared spectra, and scanning electron microscopy of impact-fractured samples showed that the soft PP phase was dispersed within the PLA matrix, and a decrease in the domain size of the dispersed phase was observed with the incorporation of MAH-*g*-PP, which acted as a compatibilizer to improve the compatibility between PLA and PP. © 2011 Wiley Periodicals, Inc. J Appl Polym Sci 121: 3223–3237, 2011

Key words: biopolymers; blends; differential scanning calorimetry (DSC); electron microscopy

INTRODUCTION

Plastics are produced mostly from petroleum feed stocks and eventually end up as nondegradable waste at the end of their service life. Disposal by incineration contributes to enormous environment pollution while reducing landfill sites. These factors have contributed to the development of environmentally friendly polymers that degrade completely under composting conditions after the end of their service life. Poly(Llactide) (PLA), an economically feasible material, among other biopolymers, namely, polycaprolactone, poly(hydroxy adipate), poly(3-hydroxybutyrate), and poly(butylene adipate-*co*-terephthalate), has gained considerable research interest for various end-use applications.[1–5] PLA has a high strength and modulus and is inherently biodegradable in nature. However, its inherent brittleness and low toughness, which are due to a low entanglement density and a high value of characteristics ratios, restricts its applications in niche markets.[6,7]

Blends of PLA with several synthetic and biopolymers have been prepared in an effort to enhance the properties of PLA. PLA blends with collagen, poly (butylenes succinate adipate), poly(ethylene glycol), poly(methyl methacrylate), polyethylene, poly(ethylene oxide), and poly(butylenes adipate-*co*-terephthalate) have been reported to improve the properties, such as toughness, modulus, impact strength, and thermal stability, compared to the neat polymer.[8,9] However, most of these polymers that are blended with PLA[10] are said to be partially immiscible and constitute multiphase blends with poor mechanical performance because of a negligible entropy of mixing. Copolymerization with other monomers and blending with immiscible or miscible polymers is a more practical and economical way of modifying PLA[11–14] to obtain improved mechanical performance. To solve the problem of immiscibility, compatibilizing agents, such as premade block or graft copolymers that are miscible with the blend components[15,16] or polymers with complementary reactive groups formed *in situ* during the melt-blending process, are used to reduce the interfacial tension and increase interface adhesion between the immiscible phases.[17,18]

Thermoplastic polyolefins have also been extensively used as toughening agents in numerous polymer blending systems, including polyester[19–21] and nylon.[22] These polymer blends, inclusive of PLA/polypropylene (PP) blends, are immiscible because of the high polarity difference between the component polymers. Over past decades, considerable efforts have been made to chemically modify polyolefin by the introduction of reactive functional

Correspondence to: S. K. Nayak (drsknayak@gmail.com).

compounds, such as PP-*g*-maleic anhydride (MAH)[23] and polyethylene-*g*-MAH,[24] to mediate the polarity at the interface. Polar-functional-group-grafted polymers can be used as compatibilizers for the interfacial modification of polymer blends and composites. The active functional group can react with numerous reactive groups to form block or graft copolymers acting as *in situ* formed or premade compatibilizers. PP-*g*-MAH has been established as an effective compatibilizer for polyolefin-based blends and composites. Mohanty et al.[25] studied the effect of PP-*g*-MAH on the interfacial properties of PP/fiber composites. The PP part of the PP-*g*-MAH is compatible with PP, and the anhydride part reacts with the fiber; this creates a favorable interface. Similar studies on maleic anhydride (MAH) and PP-*g*-MAH as compatibilizers for polyolefin-based systems[26–28] have been carried out. The role of glycidyl methacrylate (GMA) as an interfacial modifier has also been examined.[29]

In this study, the effects of MAH-*g*-PP and GMA as compatibilizing agents for PLA/PP blends were investigated. An extensive study of the influence of compatibilization on the mechanical properties and morphology of the blends was done. The thermal properties of the blends were evaluated with heat deflection temperature (HDT) testing, differential scanning calorimetry (DSC), thermogravimetric analysis (TGA), and dynamic mechanical analysis (DMA). Furthermore, the interaction of compatibilizer with the constituent polymers and the existence of interfacial bonds were studied with Fourier transform infrared (FTIR) spectroscopy.

EXPERIMENTAL

Materials

PLA (4042D), with a density of 1.24 g/cc and a molecular weight of 130,000 g/mol (M/s Cargil Dow, Bair, US-NE), was used as the base matrix. PP (Halene-P, M312) was obtained from Haldia Petrochemicals, Ltd. (West Bengal, India), with a density of 0.90 g/cc and a melt flow index of 12 g/10 min. MAH-grafted PP (MAH-*g*-PP; Epolene® G-3003), with a density 0.90 g/cc and an acid number of 47, was obtained from Eastman Chemicals (Germany). GMA, with a molecular weight of 142.16 g/mol, was supplied by Hi Media Laboratories Pvt., Ltd. (Mumbai, India). All other reagents were used without further modification.

Preparation of the blends

PLA was blended with PP at different ratios (PLA:PP = 90 : 10, 80 : 20, 70 : 30, and 50 : 50) with a batch mixer with a 69-cm^3 volumetric capacity (Haake Rheocord 9000, M/s Thermo Fisher Scientific, Germany) at temperature of 200°C with a rotor speed of 30 rpm for a duration of 7 min. Before melt blending, all the components were predried at 80°C for 12 h. Subsequently, 3 wt % compatibilizer (MAH-*g*-PP/GMA) was added to the PLA/PP blend with a 90 : 10 ratio to prepare the PLA/PP/MAH-*g*-PP and PLA/PP/GMA compatibilized blends. The mechanism is explained in Scheme 1. The blend mixtures were then cooled to room temperature and compression-molded at 190°C under 48 kg/cm^2 of pressure for a total cycle time of 15 min to fabricate sheets of 3 ± 0.1 mm thickness. Specimens were prepared with a counter–cut–copy milling machine (Ceast, Italy) as per various ASTM standards for testing and characterization.

Mechanical properties

Tensile properties

Tensile strength at yield, tensile modulus, and elongation at break were determined for samples with dimensions of 160 × 13 × 3 mm^3, with a universal testing machine (LR 100K, M/s Lloyd Instruments, UK) with a load cell of 10 kN. The test was carried out according to ASTM D 638 with a gauge length of 50 mm at room temperature and constant strain rate of 5 mm/min. A minimum of five replicate samples were tested, and the average value is reported. Corresponding standard deviations were also evaluated.

Flexural properties

The flexural modulus and strength of the compression-molded specimens with dimensions of 80 × 13 × 3 mm^3 in three-point bending mode were measured according to the ASTM D 790 in the same universal testing machine (LR 100K, M/s Lloyd Instruments, UK). The span length was 50 mm, and the crosshead speed was 1.4 mm/min at room temperature.

Impact properties

A V-notch with a depth of 2.54 mm was introduced in the specimens with dimensions of 63.5 × 12.7 × 3 mm^3 with a notch cutter. Subsequently, the measurements were carried out in an Impactometer (6545, M/s Ceast, Italy) as per ASTM D 256.

Thermal analysis

DSC

The samples were characterized to determine the glass-transition temperature (T_g), crystallization temperature (T_c), and melting temperature (T_m) of PLA

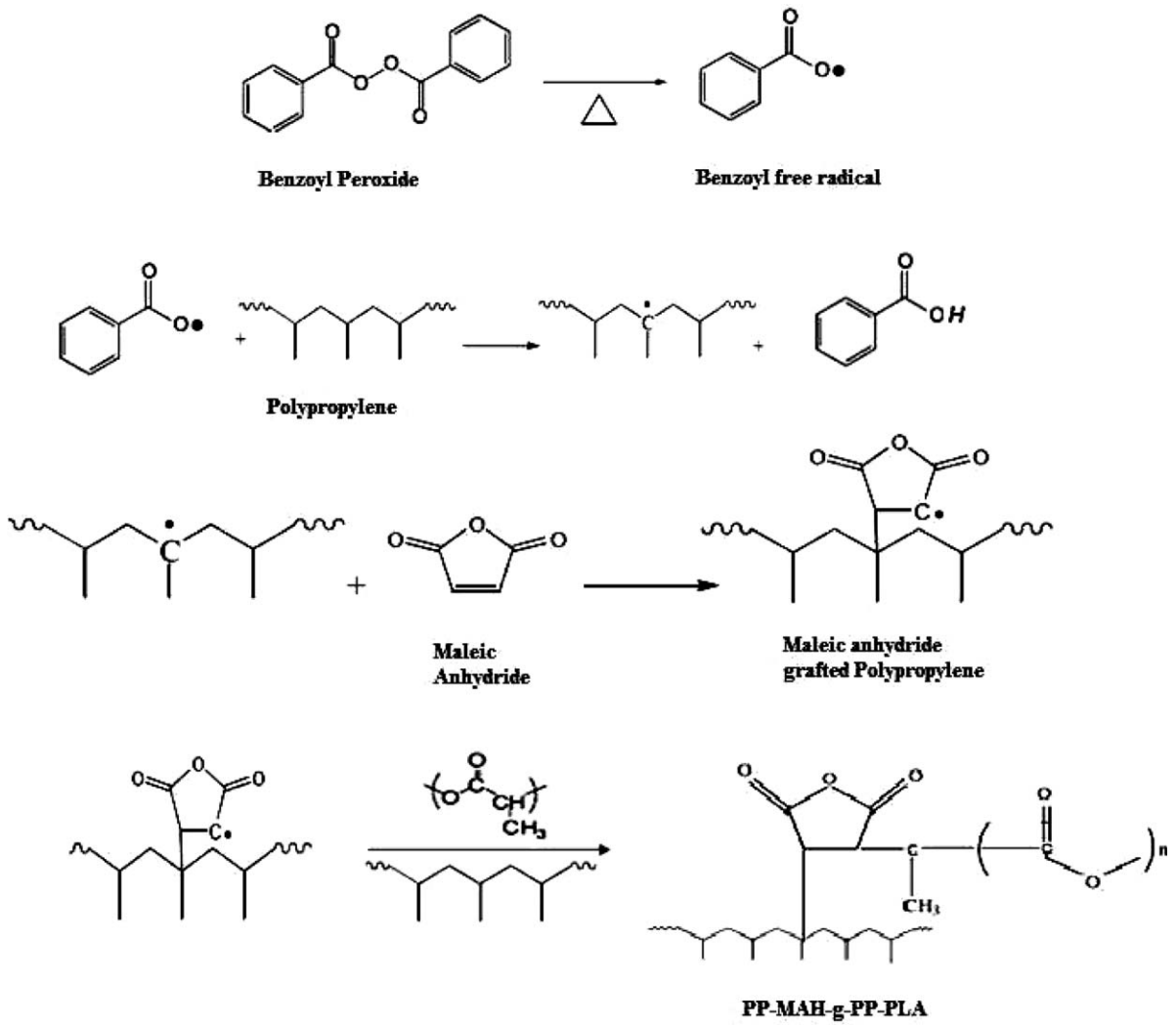

Scheme 1 Synthetic route of the PP/MAH-*g*-PP/PLA blend.

and the PLA/PP blends with and without MAH-*g*-PP/GMA. The samples were heated from room temperature to 250°C at 10°C/min in a differential scanning calorimeter (Diamond DSC, M/s Perkin Elmer, USA). Subsequently, the samples were maintained at 250°C for 10 min to remove the thermal history and then cooled to −50°C at a cooling rate of 20°C/min. The corresponding heat of fusion was recorded for calculating the degree of crystallinity (X_c; %).

TGA

Virgin PLA, PP, and their blends were subjected to TGA (Pyris-7 TG, M/s Perkin Elmer, USA) to analyze the thermal stability of the samples. Samples weighing 5–10 mg or less were heated from 40 to 600°C at a heating rate of 10°C/min under a nitrogen atmosphere. The flow rate of nitrogen was maintained at 20 mL/min. The initial degradation temperature, weight loss, and final degradation temperature (T_{fd}) of the samples were recorded.

HDT

HDTs of virgin PLA and various PLA/PP blends were determined with an HDT tester (M/s Toyoseiki Co., Japan) as per ASTM D 648. The samples were heated at a rate of 2°C/min from ambient temperature. The temperature at which the samples deflected to 0.01″ (0.254 mm) was noted as HDT.

DMA

Viscoelastic properties, such as storage modulus (E'), loss modulus (E''), and mechanical damping parameters (tan δ) as a function of temperature, were measured in a dynamic mechanical analyzer (DMA Q800, M/s TA Instruments, USA). The measurements were carried out in bending mode with a rectangular specimen with dimensions of 35 × 12 × 3 mm^3 over a temperature range of −60 to 140°C at a heating rate of 10°C/min under a nitrogen atmosphere. The samples were scanned at a fixed frequency of 1 Hz with a static strain of 0.1% and a dynamic strain of 0.1%.

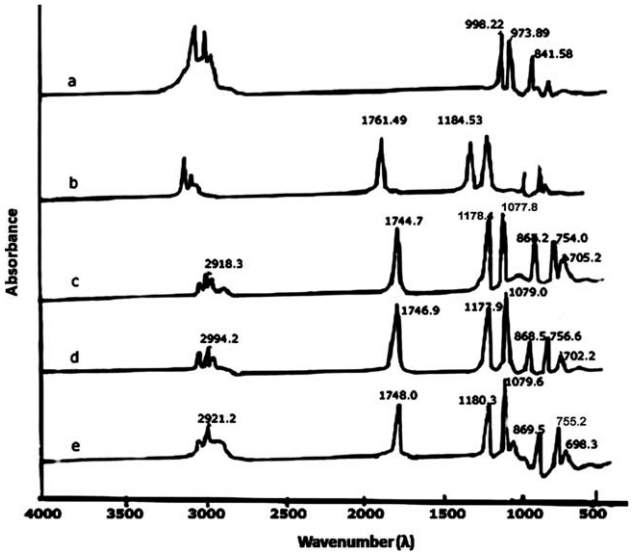

Figure 1 Comparison of the IR spectra for samples of (a) PP, (b) PLA, (c) PLA/PP blend, (d) PLA/PP/MAH-*g*-PP, and (e) PLA/PP/GMA.

Morphological investigations

Scanning electron microscopy (SEM)

The morphology of the impact-fractured samples was studies with SEM (S-3400 N, M/s Hitachi, Japan). The surface of the sample was gold-coated to avoid electrostatic charging during analysis. The interfacial characteristics of the constituent polymers were studied at a voltage of 20 kV. We evaluated the dispersion of PP in the PLA matrix by scanning the cryofractured surfaces of the specimens. In the representative zones of the scanned surfaces, the PP particle diameter was measured with Autocad software. The weight-average particle diameter (d_w) was estimated by

$$d_w = \sum n_i d_i^2 / \sum n_i d_i \quad (1)$$

where n_i is the number of particles with size d_i.

The interparticle spacing (τ) was determined from d_w and the volume fraction of the PP (ϕ_d) with Wu's model:

$$\tau = d_w[(\pi/6\varphi_d)^{1/3} - 1] \quad (2)$$

FTIR spectroscopy

FTIR spectra of PLA/PP blends with and without compatibilizers were recorded with a PerkinElmer FTIR 1720X. The spectra within the range 4000–400 cm^{-1} were observed. The interactions among the compatibilizers, PLA, and PP were studied.

RESULTS AND DISCUSSION

FTIR studies

Figure 1 depicts the FTIR spectra of virgin PP, virgin PLA, PLA/PP, PLA/PP/MAH-*g*-PP, and the PLA/PP/GMA blends. The FTIR spectrum of MAH-*g*-PP is shown in Figure 2. The absorption bands near 1792 and 1776 cm^{-1} were assigned to symmetric C=O stretching of anhydride functions grafted onto PP. Figure 1(a) shows CH_3 rocking, C—H bending, CH_2 wagging, C—C backbone stretching, and C—CH_3 stretching corresponding to PP at 998, 973, and 841 cm^{-1}. The IR spectra of PLA absorption [Fig. 1(b)] at 1761, 1184, and 1091 cm^{-1}, associated with C=O stretching, symmetric stretching of C—O—C, asymmetric CH_3, and the stretching peak of C—O—C bonds of PLA, was similar to the observations made by Wojciechowska et al.[30] Absorption peaks around 1744, 1180, 1078, 867, and 705 cm^{-1} corresponding to PLA and PP observed in the PLA/PP blend [Fig. 1(c)] indicated the absence of chemical interactions between the blend components. The disappearance of the absorption peak of the anhydride group of MAH-*g*-PP and the emergence of a new absorption signal representing the carbonyl of ester linkage stretching at 1758 cm^{-1} in the FTIR spectrum of PLA/PP/MAH-*g*-PP blend [Fig. 1(d)] indicated interaction of MAH-*g*-PP with the PLA/PP blend,[31] as explained in Scheme 1. The reaction scheme detailed in Scheme 1 follows a free-radical mechanism, wherein the peroxide initiator provides radicals, which attract hydrogen from PP tertiary carbon to form PP macroradicals. PP macroradicals combine with MAH to form MAH-*g*-PP with a free-radical site on the α carbon atom of the carbonyl group in MAH. This subsequently combines with the PLA part. Furthermore, PP is compatible with

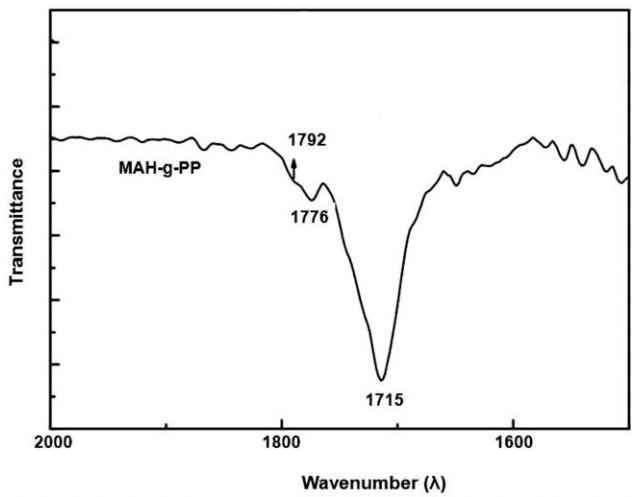

Figure 2 IR spectra of pure MAH-*g*-PP.

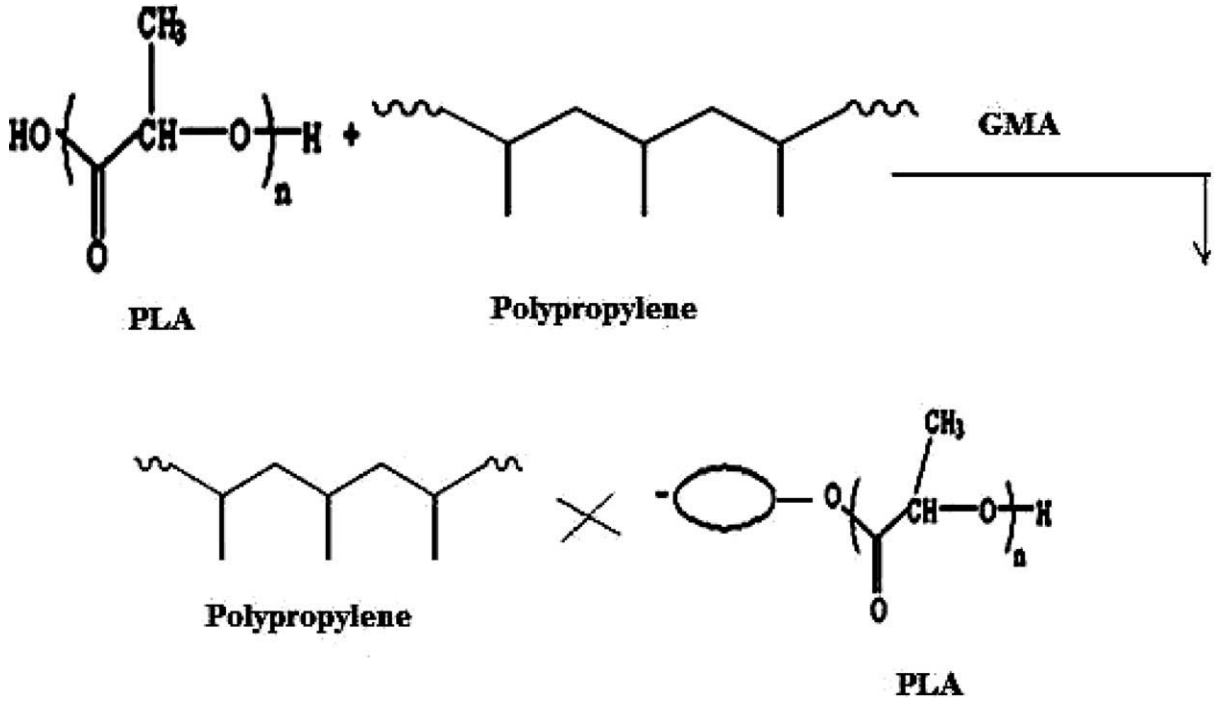

Scheme 2 Synthetic route of the PP/GMA/PLA blend.

the PP part of MAH-*g*-PP. The active site in the anhydride part of MAH-*g*-PP reacts with the carbonyl group of PLA; this results in the ester linkage. Figure 1(e) represents the FTIR spectrum of PLA/PP/GMA and shows a new peak at 698 cm^{-1} in the spectrum, which was attributed to the presence of any unreacted unsaturated alkene group in GMA and indicates the absence of any successful interaction (Scheme 2). As shown in Scheme 2, GMA reacts only with the PLA component, whereas it shows no interaction with PP.

Mechanical properties of the PLA/PP blends

Effect of the blend compositions on the mechanical properties of the PLA/PP blends

Tensile properties. The tensile properties of virgin PLA and its blends are depicted in Table I. It is evident that the virgin matrix displayed a tensile strength of 48.71 MPa, with a tensile modulus of 1254 MPa and a percentage strain at break of 2.69%. The incorporation of PP matrix to the tune of 10–70 wt % within the PLA matrix resulted in a decreased tensile strength in the resultant blends. This was probably due to incompatibility of hydrophobic PP with polar PLA or to the high polarity difference between the constituent polymers, which resulted in sharp boundaries between the two polymeric phases and led to the formation of voids and microcracks when the samples were subjected to constant deformation.[31]

However, the tensile modulus and stress at break of the blend increased at the blend ratio of 90 : 10, to the tune of 11 and 18%, respectively, compared to those of virgin PLA. PP incorporated within the PLA matrix probably acted as a reinforcing agent, which contributed to enhancing the modulus and stress at break in the case of the PLA/PP blend. Conversely, a decreasing trend in the tensile modulus was observed with increases in the PP content beyond 10 wt % in the blend system. This phenomenon was attributed to the increase in the extent of incompatibility between the constituents with increasing amount of PP.

The percentage elongation at break did not show any appreciable increase at 10–30 wt % PP content. However, beyond 30 wt % PP, the percentage elongation increased; this revealed the change of failure mode from brittle to ductile.[32] With the incorporation of PP above 50 wt %, PP formed a continuous phase with PLA domains dispersed within the matrix.

Flexural properties. The variation of the flexural properties of the PLA/PP blend as a function of PP content is enumerated in Table I. Virgin PLA showed a flexural strength of about 13.2 MPa, which tended to increase in the PLA/PP blends with 10 wt % PP. This behavior was probably due to the plasticizing effect of PP within PLA, which is brittle in nature. However, the addition of PP beyond 10 wt % led to decreases in the flexural strength and flexural modulus and indicated a phase-separated morphology in the immiscible PLA/PP blends.

TABLE 1
Effect of Blend Compositions on the Mechanical Properties of PLA

Compositions	Tensile Strength (MPa)	Nicholais-Narkis model (MPa)	Porosity model (MPa)	Tensile Modulus (MPa)	Einstein model (MPa)	Guth's model (MPa)	Stress at break (%)	Elongation at break (%)	Flexural strength (MPa)	Flexural modulus (MPa)	Impact strength (J/m)
V-PLA	48.71 ± 7.0	48.71	48.71	1254.26 ± 55.0	1254.266	1254.266	12.76 ± 0.4	2.69 ± 0.25	13.2 ± 4.0	4185 ± 73.0	21.09 ± 5.0
V-PP	27.24 ± 4.5	–	–	983.31 ± 13.0	–	–	8.69 ± 0.85	16.39 ± 0.46	11.2 ± 8.0	1000 ± 43.0	98.17 ± 9.0
PLA/PP(90/10)	37.12 ± 4.0	33.37	45.58	2302.8 ± 16.0	1420.785	1982.28	37.08 ± 4.0	1.87 ± 0.32	17.32 ± 7.0	2952 ± 70.0	24.81 ± 4.0
PLA/PP(80/20)	26.99 ± 0.5	24.94	42.85	1720.6 ± 43.0	1575.607	3218.429	19.25 ± 0.5	2.80 ± 0.09	15.98 ± 5.0	2417 ± 42.0	18.20 ± 1.0
PLA/PP(70/30)	18.30 ± 0.6	18.27	40.46	1865.32 ± 17.0	1719.922	4855.987	17.73 ± 0.7	2.36 ± 0.57	13.95 ± 5.0	2081 ± 67.0	21.24 ± 5.0
PLA/PP(50/50)	12.63 ± 0.6	7.75	36.46	1543.07 ± 17.0	1981.037	9008.98	6.32 ± 4.0	3.43 ± 0.86	14.25 ± 4.0	1611 ± 52.0	39.93 ± 4.0
PLA/PP(30/70)	14.65 ± 0.3	0.00	33.26	1249.66 ± 7.0	2210.947	13934.74	7.14 ± 3.0	27.82 ± 4.0	15.22 ± 1.0	1896 ± 10.0	40.43 ± 8.0

*Note: V-PLA = virgin PLA; V-PP = virgin PP.

Impact properties. The effect of PP content on the notched Izod impact strength of the PLA/PP blends of various compositions at room temperature is given in Table I. It was evident that virgin PLA displayed an impact strength of 21.09 J/m, which increased to 24.81 J/m in the case of the blend with 10 wt % PP. Beyond 10 wt % PP, there was a significant decrease in the impact strength of the blend. The blends prepared at PLA/PP ratios of 80 : 20 and 70 : 30 exhibited a decrease in the impact strength to the tune of 26 and 14.7%, respectively. The solubility parameters of PLA and PP were 9.7 and 16.8 $MPa^{1/2}$, respectively. This difference might have contributed to the immiscible characteristics between the component polymers and, thereby, decreased the impact properties. However, with the increase in PP content beyond 30 wt %, there was an increase in the impact strength of the blends compared to virgin PLA. This behavior was probably due to the high impact strength of the virgin PP matrix (98.97 J/m), which contributed to an enhancement in the absorbing impact energy in the blends. At a 50 : 50 ratio of PLA/PP, there was an increase in the impact strength of virgin PLA from 21.09 to 39.93 J/m. Similarly, blends with 70 wt % PP exhibited an optimum impact strength of 40.43 J/m. However, in all cases wherein the PP part was a major component, it formed a continuous phase with PLA domains as a dispersed phase, and the impact strength was lower compared with the PP matrix. This further confirmed that PLA and PP are incompatible in blends.[30]

Micromechanical modeling

Tensile strength. To investigate the discontinuity in the blend system, the tensile strength data were compared with the Nicholais–Narkis (N–N) model (Table I) and porosity model (P model).[33,34] These models have been used in two-phase polymer blends/composites to study the discontinuities in the system. The tensile strength is proportional to the area fraction or volume fraction of the discontinuous phase.[35–37]

In the N–N model, the area of fraction is considered operative.[38] The weightage factor (K) describes the blend/composite structure. For hexagonal packing of the dispersed phase in the plane of highest density, $K = 1.1$,[39] and those with no adhesion in the presence of a spherical dispersed phase ($K = 1.21$). $K = 1$ stands for the absence of stress concentration, and when the dispersed phase did not weaken the structure, $K = 0$. The value of K indicates the interphase adhesion; the lower the value of K is, the better the adhesion will be:[34]

$$\sigma_b/\sigma_m = (1 - K\varphi_d^{2/3}) \quad (3)$$

where $K = 1.21$, σ_b is the tensile strength of the blends, σ_m is the tensile strength of virgin PLA, and ϕ_d is the volume fraction of PP.

In the P model, the discontinuous phase was considered equivalent to voids or pores that affected the mechanical properties of the two-phase systems[39] on account of nonadhesion at the phase boundaries. The parameter α describes the stress concentration in the structure:

$$\sigma_b/\sigma_m = \exp(-\alpha\varphi_d) \quad (4)$$

where $\alpha = 0.55$.

Experimentally determined values of the corresponding tensile strength versus ϕ_d per the N–N model and P model and are represented in Table I. It is evident from the Table 1 that the experimentally determined values of the tensile strength showed a positive deviation compared with the theoretical values of the N–N model. This may have been due to the little bit of interaction between PLA and PP in the blends. Furthermore, in case of the P model, the experimentally determined values of the tensile strength showed a negative deviation compared with the theoretical values of the P model with the incorporation of PP. This decrease in the tensile strength may have been due to a change in the effective cross-sectional area brought about by the dispersed phase, as PLA/PP blends are incompatible in nature, which results in sharp boundaries between the two polymeric phases and leads to the formation of voids and microcracks when the samples are subjected to constant deformation.

Tensile modulus. To investigate and compare the tensile modulus of the blend system, two models were used, namely, the Einstein model and Guth's model (Table I). In case of poor adhesion, where the polymer matrix slips by the filler particles,[40] the Einstein Eq. (5) was used:

$$E_b = E_m(1 + \varphi) \quad (5)$$

where ϕ is the volume fraction of the particles and E_m and E_b are the Young's moduli of the matrix and composite, respectively.

To explain the reinforcing effect of colloidal fillers, Guth and Gold[41] introduced a quadratic term, which is a modified form of the Einstein equation and is represented as Eq. (6). It is used to find the interaction between filler particles:

$$E_b = E_m(1 + 2.5\varphi + 14.1\varphi^2) \quad (6)$$

where ϕ is the volume fraction of the filler.

It is evident from Table I that an increase in the experimental values of the tensile modulus was shown with an increase in PP compared with the theoretical values shown by the Einstein model. This may have been because the PP incorporated within the PLA matrix probably acted as a reinforcing agent, which contributed to enhancing the interfacial interaction and led to an enhancement in the modulus. However, a decrease in the experimental values of the tensile modulus was shown with an increase in PP content when compared with the theoretical values shown by Guth's model. This phenomenon was attributed to the increase in the extent of incompatibility with increasing amount of PP.

Factors influencing the reactivity of MAH-*g*-PP and GMA on the PLA/PP blends

As evident from Table I, the PLA/PP blend compositions showed characteristics of immiscible and multiphase blends with poor mechanical performance. The mechanical test results discussed in earlier sections indicated that PLA/PP blends at a 90 : 10 ratio exhibited optimum tensile modulus and stress performance values. Hence, this composition was retained for further studies to investigate the effect of the addition of reactive compatibilizers, GMA and MAH-*g*-PP, on the interface and properties of the blends. To enhance the mechanical properties of a blend, the compatibility between two phases has to be increased. In this context, both PLA and PP were incompatible polymers, which showed the formation of a biphase morphology at the interface in all compositions. The mechanism of action of GMA is depicted in Scheme 2. Furthermore, PLA, being a brittle polymer, is difficult to process and to improve the processability of PLA while retaining its inherent biodegradability characteristics; a minimum quantity of PP was added.

Tensile properties. The tensile properties with and without compatibilizers are tabulated in Table II. It was evident that the tensile strength increased from 37.12 to 46.32 MPa, by 19.8%, with the incorporation of 3 wt % MAH-*g*-PP compared to that of the uncompatibilized blend and was almost comparable with virgin PLA. However, the tensile modulus increased marginally to 6% in the presence of MAH-*g*-PP, which was probably because the interfacial adhesion level had no influence on the low-strain tensile properties.[42] Nevertheless, the percentage stress at break and percentage strain at break increased to the tune of 20 and 29%, respectively, compared to those of the uncompatibilized blend. This increment in the tensile properties was attributed to the improved interfacial interaction between PLA and PP. The anhydride group of MAH-*g*-PP reacted with the carbonyl group of PLA, and the PP part of the

TABLE II
Effect of the Compatibilizers on the Tensile Properties of the Optimized Blend

Composition	Tensile strength (MPa)	Tensile modulus (MPa)	Stress at break (%)	Strain at break (%)
V-PLA	48.71 ± 7.0	1254 ± 55.0	12.76 ± 0.4	2.69 ± 0.25
V-PP	27.25 ± 4.5	983.31 ± 13.0	8.69 ± 0.85	16.39 ± 0.46
PLA/PP (90 : 10)	37.12 ± 4.0	2302 ± 16.0	37.08 ± 4.0	1.87 ± 0.32
PLA/PP (90 : 10) + 3% MAPP	46.33 ± 1.46	2433 ± 21.0	46.309 ± 1.44	2.617 ± 0.31
PLA/PP (90 : 10) + 3% GMA	35.22 ± 2.13	2050 ± 68.0	33.429 ± 2.76	2.22 ± 0.41

*Note: V-PLA = virgin PLA; V-PP = virgin PP.

compatibilizer became compatible with PP. Thus, MAH-*g*-PP effectively reduced the interfacial tension between PLA and PP and, thus, resulted in improved compatibilization and more shear yield during testing.

Conversely, decrease of 5% in tensile strength, 12% in tensile modulus, and 11% in stress at break were observed with the incorporation of 3 wt % GMA. This was probably due to the incompatibility of GMA with the PLA/PP blend. The epoxy group of GMA formed an ester linkage via the carbonyl group of PLA, whereas no such linkage or interaction of GMA was seen with PP, as evident from FTIR studies discussed later.

Flexural properties. The modified interface influenced the flexural strength and flexural modulus. The MAH-*g*-PP incorporated blend showed an increase in strength from 17.32 to 32.6 MPa to the tune of 47%. The soft PP phase present in the matrix and MAH-*g*-PP increased the dissipation of stress energy through the modified interface. The flexural strength was also positively affected by 3 wt % GMA, with an increase from 17.32 to 22.27 MPa, by 28.5%, in comparison with the uncompatibilized blend.

The flexural modulus of the PLA/PP blend exhibited a marginal decrease from 2952 to 2740 and 2920 MPa with the incorporation of MAH-*g*-PP and GMA, respectively. This may have been due to the formation of a soft phase at the interface region. PP reduced the stiffness of virgin PLA because of the associated reduction in the effective cross-sectional areas of the samples, which resulted in the reduction of property values, as shown in Table III.

Impact properties. An increase in the impact strength, by 17%, from 25 to 29 J/m, was observed with the incorporation of 3 wt % MAH-*g*-PP; this may have been due to improved interaction of MAH-*g*-PP with the PLA/PP blend interface, which led to a better dispersion of PP within the PLA matrix (Table III). This further result in the reduction of particle size of the dispersed-phase PP, which is cited from the SEM studies discussed in later sections, led to an enhancement in the compatibility with decreasing interfacial tension.

The impact strength was found to decrease by 6%, from 25 to 23.3 J/m, with the incorporation of GMA in the blend ratio; this was probably due to an increase in the stress concentration level, as there was no specific interaction of GMA with the PLA/PP blend.

Stress–strain characteristics

Figure 3 shows the stress–strain curve of virgin PLA, PP, and the uncompatibilized and compatibilized PLA/PP blends. To improve the mechanical properties, T_g must be lower than the testing temperature. If T_g is lower than the testing temperature, the mobility of chain segments increases, and the chains can move more easily.[43] The high modulus and low percentage strain at break of about 1254 MPa and 2.69%, respectively, of virgin PLA confirmed hard and brittle characteristics, whereas PP exhibited a lower modulus and high percentage strain at break; this indicated a ductile nature. With

TABLE III
Effect of the Compatibilizers on the Flexural and Impact Properties of the Optimized Blend

Composition	Flexural strength (MPa)	Flexural modulus (MPa)	Impact strength (J/m)
V-PLA	13.2 ± 4.0	4185.45 ± 73.0	21.09 ± 5.0
V-PP	11.2 ± 8.0	1000 ± 43.0	98.17 ± 9.0
PLA/PP (90 : 10)	17.32 ± 7.0	2952 ± 70.0	24.82 ± 4.0
PLA/PP (90 : 10) + 3% MAPP	32.60 ± 10.0	2740 ± 77.0	28.76 ± 3.5
PLA/PP (90 : 10) + 3% GMA	22.27 ± 8.0	2920 ± 58.0	23.36 ± 4.0

*Note: V-PLA = virgin PLA; V-PP = virgin PP.

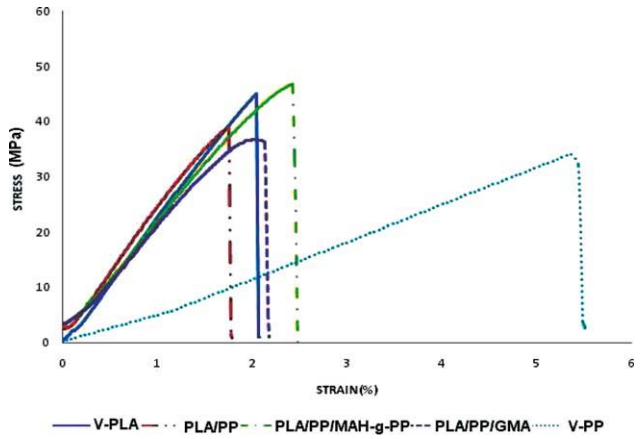

Figure 3 Stress-strain curve for PLA, PP, PLA/PP, PLA/PP/MAH-*g*-PP, PLA/PP/GMA blends. [Color figure can be viewed in the online issue, which is available at wileyonlinelibrary.com]

the incorporation of 10 wt % PP into the PLA matrix, the percentage stress increased with a corresponding increase in the modulus. This represented a change in the failure mode from brittle to ductile. However, elongation did not show any dramatic change in comparison to virgin PLA because only a small amount of PP was incorporated in the brittle PLA. Furthermore, with the incorporation of 3 wt % MAH-*g*-PP in the blend, there were increases in the modulus and percentage stress at break to 2433 MPa and 46.309%, respectively, which may have been due to enhancements in the interfacial interaction of PLA with PP. The compatibilizer plays a role like a bridge in the blend system, decreasing the phase boundary between the polymers and improving the miscibility of the blend, as discussed by Chenget et al.[44] Similarly, the incorporation of 3 wt % GMA also showed an increase in the modulus but to a somewhat extent lesser in comparison to the MAH-*g*-PP compatibilized blend; this was probably due to a lack of specific interaction of GMA with PP.

Morphological investigation

SEM

SEM micrographs of the impact-fractured surfaces of the PLA/PP (90 : 10) blends are illustrated in Figure 4(a). The phase separation between the continuous PLA phase and dispersed PP phase is clearly shown

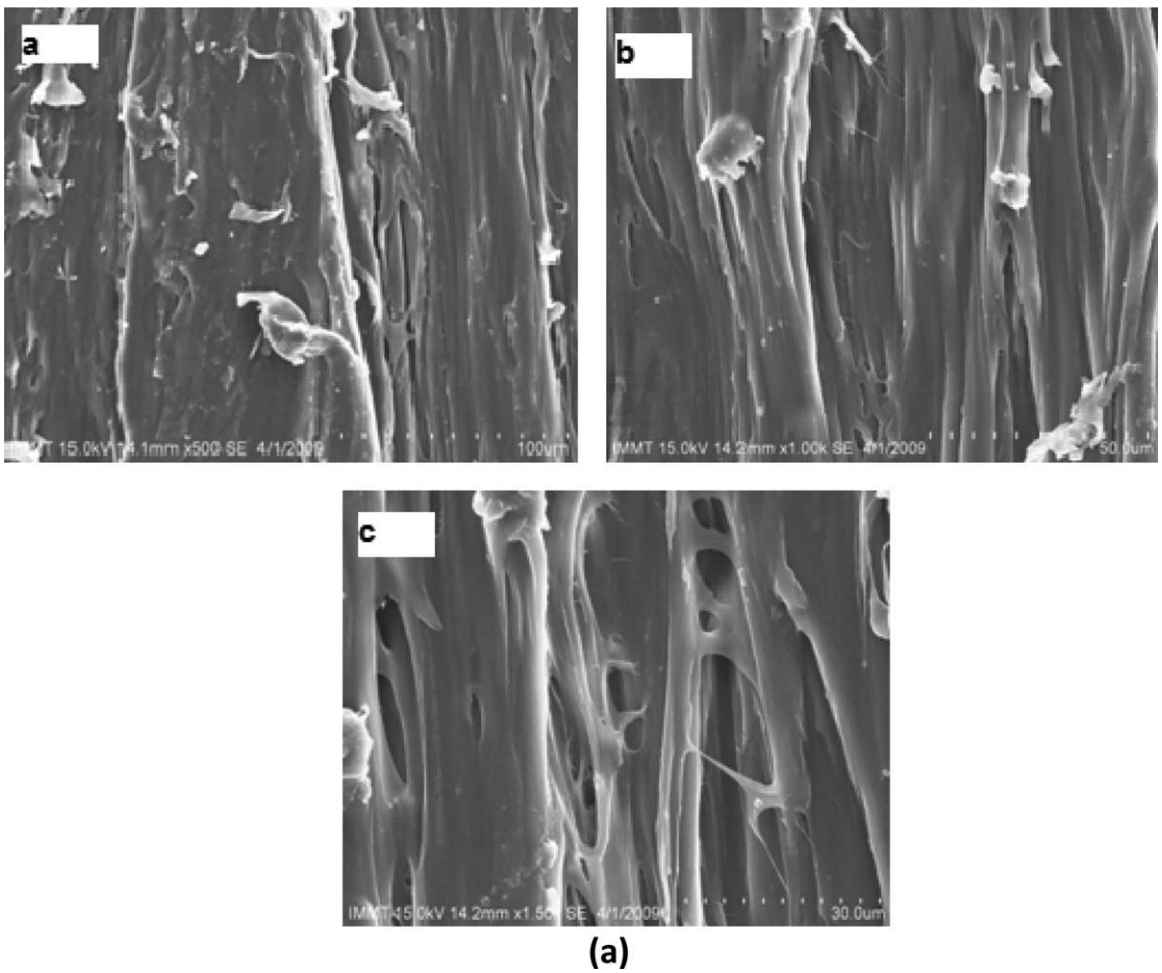

Figure 4a SEM micrographs of PLA/PP (90/10) blend at (a) 100 μm, (b) 50 μm, (c) 30 μm.

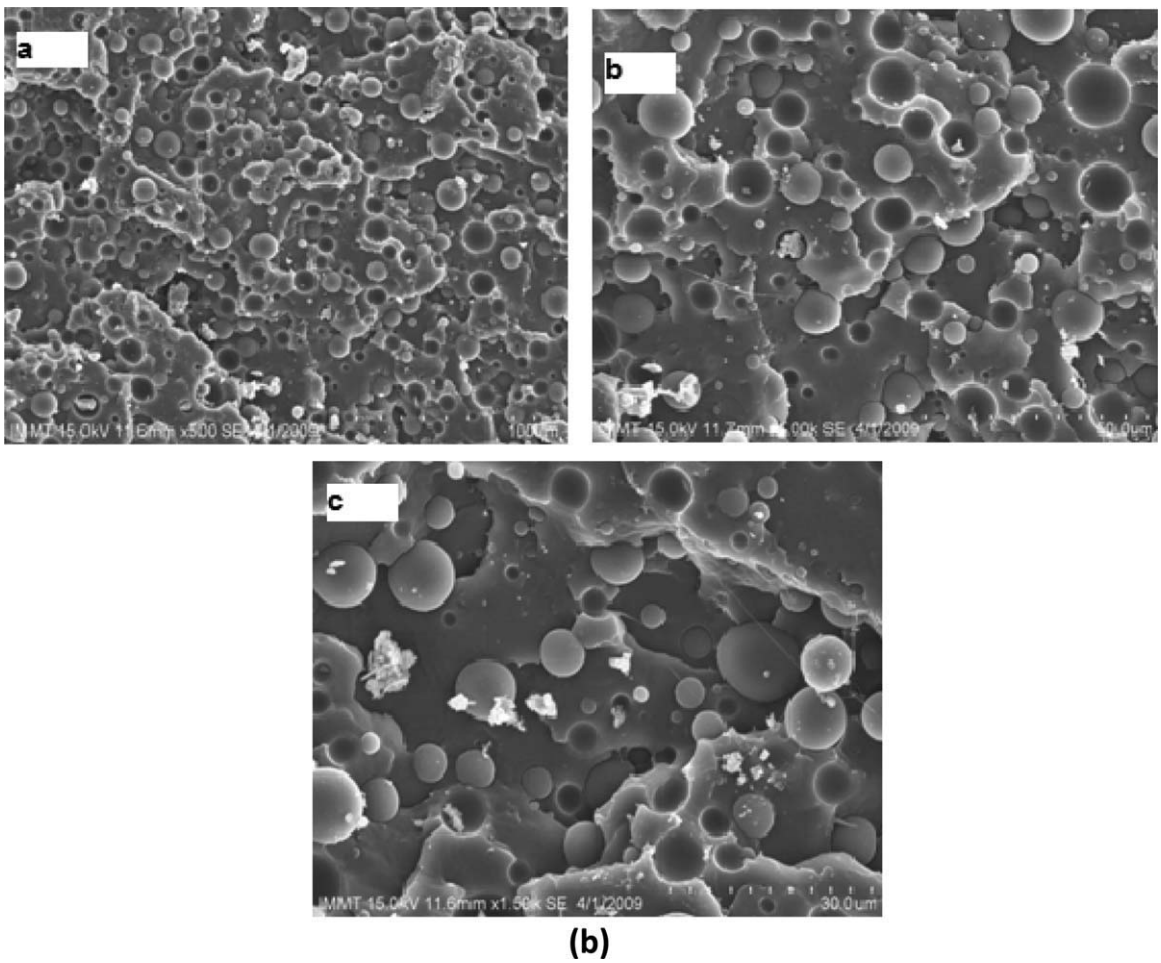

Figure 4b SEM micrographs of PLA/PP (90/10) + 3%MAPP as a compatibilizer at (a) 100 μm, (b) 50 μm, (c) 30 μm.

in the figure. The micrograph reveals a distinct two-phase morphology with the PP phase dispersed evenly within the PLA matrix. The fine pin holes visible in the micrographs clearly indicate that PP phase separated out during the application of impact force because of the immiscibility of the blend components.[31]

Figure 4(b) represents SEM micrographs of the PLA/PP/MAH-*g*-PP blends at different magnifications. It can be observed that the incorporation of MAH-*g*-PP in the blend led to improved miscibility and reduced the interfacial tension between PLA and PP.[30] The particle size of the dispersed phase was also found to decrease with compatibilization. The SEM micrographs of the PLA/PP blends compatibilized with GMA [Fig. 4(c)] showed randomly distributed PP within PLA matrix.

The particle size of the PLA/PP blend components could not be calculated. The average particle size of the GMA compatibilized blends was observed to be 9.16 μm. This indicates the absence of any favorable interaction between GMA and the component polymers, as observed in the FTIR studies and which was already discussed in an earlier section. Furthermore, the average particle size of PLA/PP/MAH-*g*-PP was calculated to be 5.82 μm, which was lower as compared to that of the GMA-compatibilized blend. A decrease in the particle size upon compatibilization, even to the submicrometer level, was observed by Ravikumar and Ranganathaiah[45] for poly(trimethylene trephthalate) (PTT)/maleinized ethylene propylene diene monomer (EPDM) blends and Arvind et al.[46] for PTT/linear low-density polyethylene blends.

DMA

E′

The temperature dependence of *E′* of PLA, PP, and the PLA/PP blends is depicted in Figure 5. *E′*, obtained from DMA, is closely related to the load-bearing capacity of the material, and when the experiment is carried out in three-point bending mode, it is analogous to the flexural modulus measured per ASTM D 790.[47]

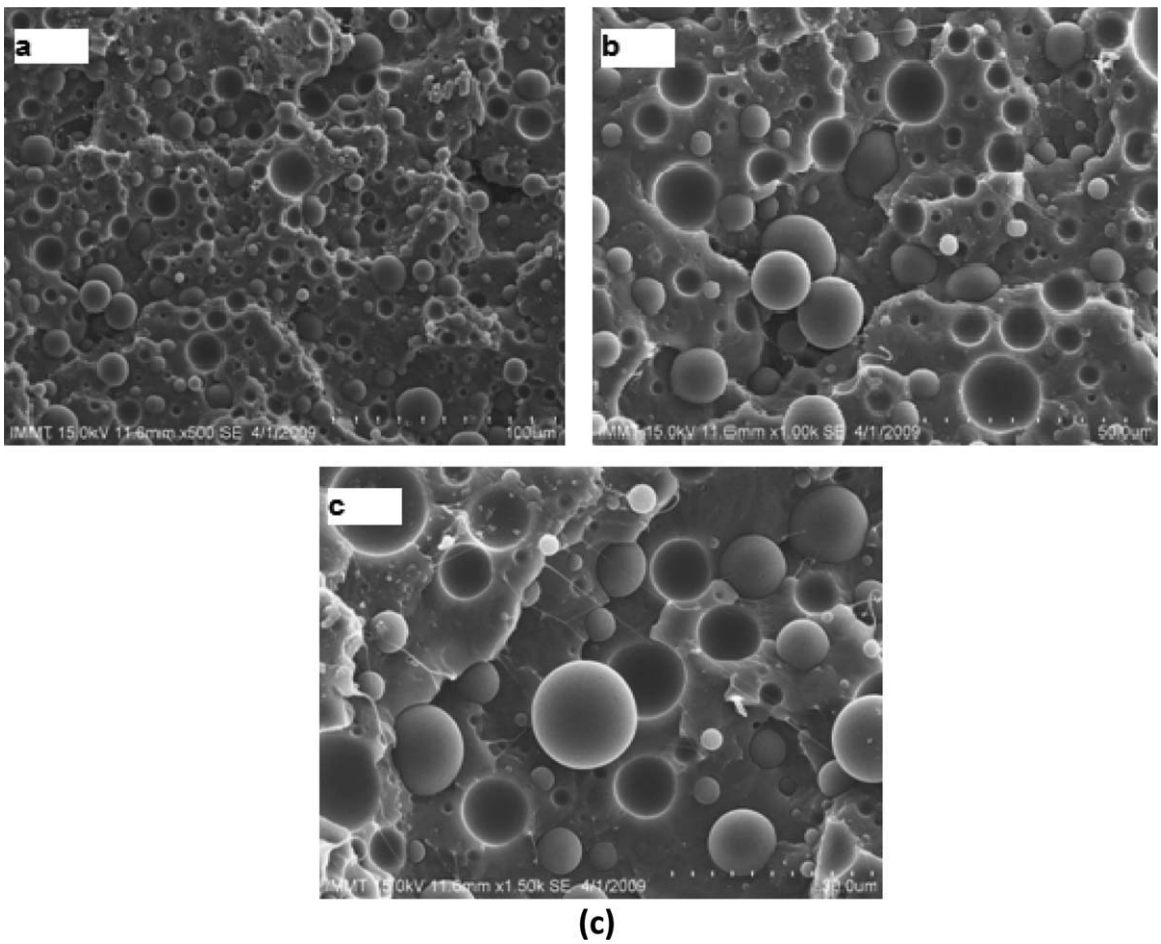

Figure 4c SEM micrographs of PLA/PP (90/10) +3%GMA as a compatibilizer at (a) 100 μm, (b) 50 μm, (c) 30μm.

The incorporation of 10 wt % PP resulted in the reduction of E' of the virgin PLA polymer. This decrease was attributed to the presence of a soft PP phase, which decreased the crystallinity and stress level of the virgin matrix. However, the addition of MAH-*g*-PP had a positive effect on E', which exhibited an increase of 8% at 30°C. The phase boundary between the incompatible constituents was modified by MAH-*g*-PP and, thus, allowed efficient stress transfer at the interface. The plasticizing effect of GMA, which turned the blend to a soft phase, resulted in no appreciable change in E', as expected. In the case of virgin PLA, the rate of fall of the matrix modulus was significant around 60°C, which was probably the T_g region of the matrix. However, in case of the blends, the T_g shifted to a higher transition, which was found to be maximum in case of the PLA/PP/MAH-*g*-PP blends. This phenomenon was primarily due to the reinforcing effect of the MAH-*g*-PP, which contributed to an effective stress transfer to the matrix at the interface. This indicated a higher thermal stability in the blends.

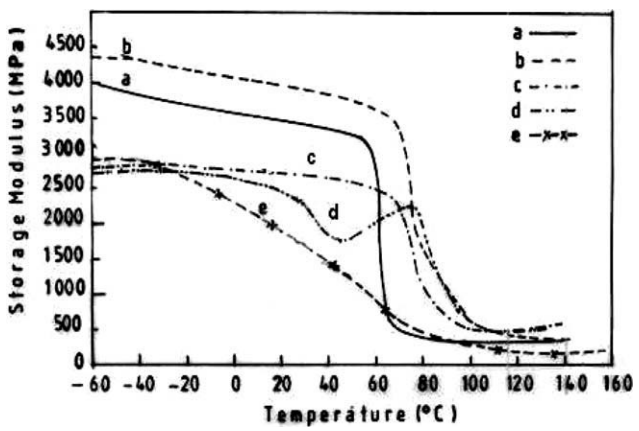

Figure 5 Variation of storage modulus with temperature for a) PLA, b) PLA/PP/MAH-*g*-PP, c) PLA/PP/GMA, d) PLA/PP, e) PP.

E″

PLA showed a sharp transition around 61.88°C corresponding to its T_g, whereas PP showed two different transitions around 23.58°C (β transition), corresponding to its T_g, and 95.79°C (α transition), related

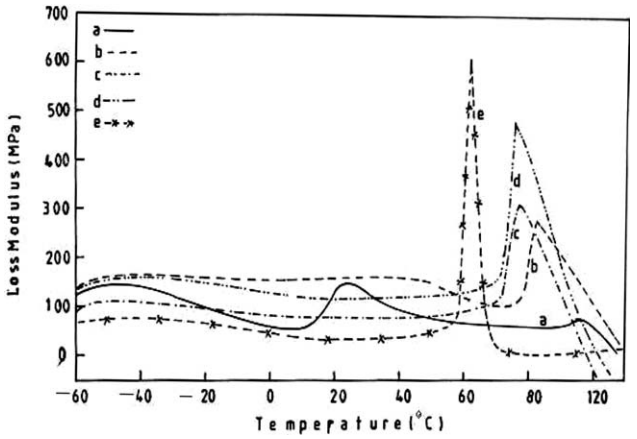

Figure 6 Variation of loss modulus with temperature for a) PP, b) PLA/PP, c) PLA/PP/GMA, d) PLA/PP/MAH-*g*-PP, e) PLA.

to the crystallite melting, shown in Figure 6. The PLA/PP blend with 10 wt % PP showed two different transitions around 27 and 85°C. The high-temperature peaks were probably associated with the T_g of PLA and the low-temperature peak of PP. This confirmed the formation of a biphase structure in the blend. With the incorporation of MAH-*g*-PP, the T_g of PLA was shifted to a higher value of 75.61°C, and a weak transition, as compared to the uncompatibilized blend, was observed at 17.59°C, corresponding to the T_g of PP. A similar trend was observed for the PLA/PP/GMA blend. The E'' values of the PLA/PP/MAH-*g*-PP and PLA/PP/GMA blends were observed to be 479.4 and 325.0 MPa, respectively. The higher modulus of the MAH-*g*-PP compatibilized blend exhibited its improved interfacial stability compared to GMA. This further indicated the reinforcing effect of MAH-*g*-PP, which restricted the segmental motion of the matrix chain.

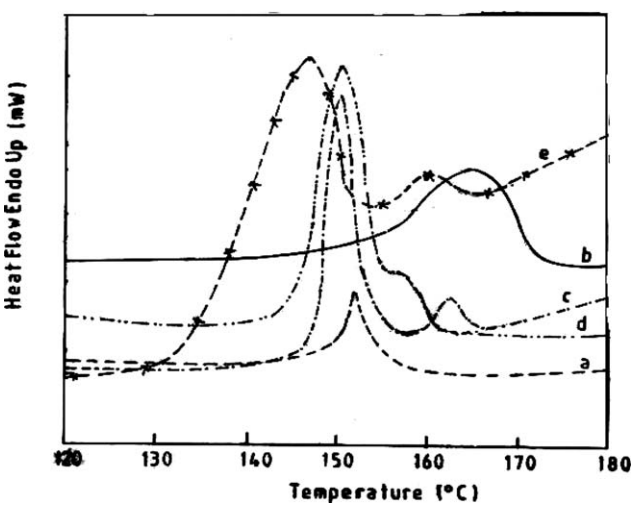

Figure 7 DSC melting thermograms of a) PLA, b) PP, c) PLA/PP (90/10), d) PLA/PP/MAH-*g*-PP, e) PLA/PP/GMA.

Thermal properties

DSC

DSC heating and cooling thermograms, illustrating the melting and crystallization behaviors of PLA, PP, and the PLA/PP compatibilized blend systems, are depicted in Figures 7 and 8. It is evident that the DSC thermogram of virgin PLA shows a single sharp endothermic peak, revealing characteristic T_m of the matrix polymer around 151°C, whereas that of PP shows a broad T_m around 164°C. The PLA/PP blend also revealed a similar melting range, corresponding to the PLA matrix. However, two distinct melting peaks around 150 and 165°C, corresponding to that of PLA and PP, respectively, were observed in the blend; this indicated a phase-separated morphology, which was in agreement with the SEM studies. In the case of the PLA/PP blend compatibilized with MAH-*g*-PP, the melting transition of PP broadened and became cocontinuous with that of PLA. This opened up a miscibility window between the two incompatible polymers. Conversely, the transition peak became more prominent with the incorporation of GMA as a compatibilizer; this, thereby, confirmed insufficient interaction between the two polymers with GMA at the interface. Also, a marginal decrease in T_m was observed, which could be attributed to the small decrease in lamellar thickness.[30]

T_m values of crystalline polymers can be related to the size and perfection of crystal units. T_m, T_c, and

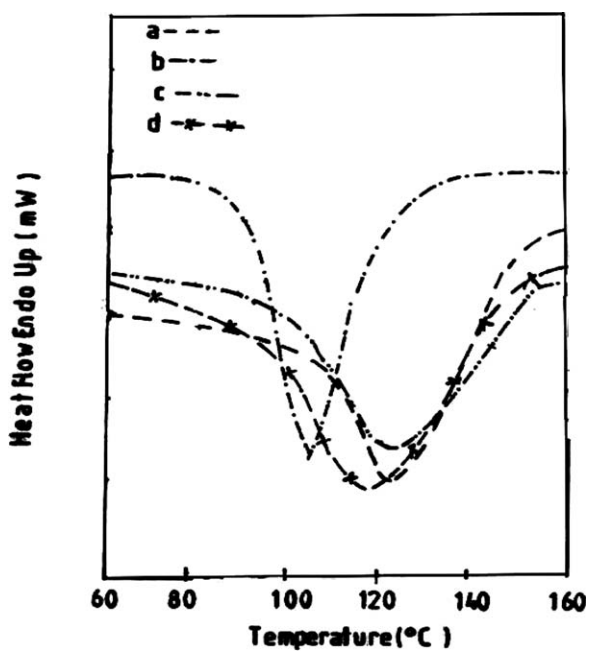

Figure 8 DSC crystallization thermograms of a) PLA/PP/MAH-*g*-PP, b) PP, c) PLA/PP, d) PLA/PP/GMA.

TABLE IV
DSC Analysis of PLA, PP, and the PLA/PP Blends

Compositions	T_g (°C)	T_c (°C)	T_m (°C)	ΔH_m (J/g)	X_{cblend} (%)	X_{cPLA} (%)
V-PLA	61.68	113	151.02	—	33	33
V-PP	—	106.57	164.82	41.87	—	—
PLA/PP (90 : 10)	61.60	124.18	150.42	13.08	15.52	13.97
PLA/PP (90 : 10) + 3% MAPP	60.07	124.41	150.65	16.77	20.25	17.92
PLA/PP (90 : 10) + 3% GMA	55	117.97	146.91	9.45	11.40	10.09

*Note: V-PLA = virgin PLA V-PP = virgin PP.
ΔH_m is enthalpy melting.

heat of fusion are represented in Table IV. Crystallization peaks could not be obtained for virgin PLA in this investigation. Lewitus et al.[48] reported that PLA showed a weak transition at 112°C, closer to that of PP, which exhibited a sharp transition corresponding to T_c at 106.57°C. As evident from the crystallization thermogram T_c, the transition had an outward shift, which indicated an increase in T_c after blending. The single transition noted for the blend samples may likely have been due to the overlapping of the peaks of the constituent polymers. The incorporation of PP within the PLA matrix increased T_c of the virgin polymer from 112 to 124.18°C. Furthermore, the PLA/PP blends compatibilized with MAH-*g*-PP also showed a single transition at 124.41°C, thus revealing that T_c remained constant, regardless of the addition of MAH-*g*-PP. Conversely, with the incorporation of GMA, T_c showed only a marginal increase, to 117°C, as compared with the neat polymer; this indicated a lack of favorable influence of GMA on improving the compatibility of PLA and PP.

The X_c (%) values of PLA and its blends are displayed in Table IV. X_c of 100% crystalline PLA was taken to be 93.6 J/g on the basis of the studies carried out by Lewitus et al.[48] It was evident that X_c of PLA decreased with the incorporation of even a small quantity of PP, that is, 10 wt %, which was probably due to the increase in the amorphous region between the lamellae, which, thus, inhibited the crystallization process of PLA.[49] A further increase in X_c was obtained with the incorporation of MAH-*g*-PP within the blend composition. This was probably due to the modified interface of PLA/PP with the incorporation of MAH-*g*-PP.

TGA

The thermal stabilities of the virgin PLA, PP, and PLA/PP blends evaluated by TGA are represented in Table V and Figure 9. As evident from Table V, PP was thermally more stable than PLA. The onset temperature of thermal degradation (T_{10}) of PLA was 352°C, whereas PP started to degrade at 374°C. The incorporation of 10 wt % PP resulted in the decrease of T_{10} of PLA to 374°C in the blend. Similarly, the temperature at 50% weight loss (T_{50}) also decreased in the case of the blend to 369°C, as compared with that of the neat polymer (389°C). Both T_{10} and T_{50} had an increase in magnitude with the addition of MAH-*g*-PP as a compatibilizer. The physical and chemical bonding between MAH-*g*-PP and the polymers resulted in an enhancement in the thermal stability.[50] Conversely, the incorporation of GMA led to decrease in T_{10} and T_{50}; this indicated the absence of any reaction taking place within the blend constituents. T_{fd} also increased from 420°C for virgin PLA to 465°C for PLA/PP blend which was decreased to 450°C and 460°C with the incorporation of compatibilizers MAH-*g*-PP and GMA within the blend matrix.

Heat distortion temperature

The HDT values for PLA, PP, and PLA/PP are tabulated in Table V, which shows that the incorporation of PP to the tune of 10 wt % increased the HDT of PLA from 68 to 72.3°C. Furthermore, the addition of MAH-*g*-PP resulted in an additional increase in HDT of the PLA matrix in the blend to 79°C. This further confirmed the reduced interfacial tension in

TABLE V
Thermal Properties of PLA, PP, and the PLA/PP Blends

Composition	T_{10} (°C)	T_{50} (°C)	T_{fd} (°C)	HDT (°C)
V-PLA	352	389	420	68
V-PP	374	429	480	88
PLA/PP (90 : 10)	337	369	465	72.3
PLA/PP (90 : 10) + 3% MAPP	345	373	450	79.8
PLA/PP (90 : 10) + 3% GMA	320	361	460	74.0

*Note: V-PLA = virgin PLA; V-PP = virgin PP.

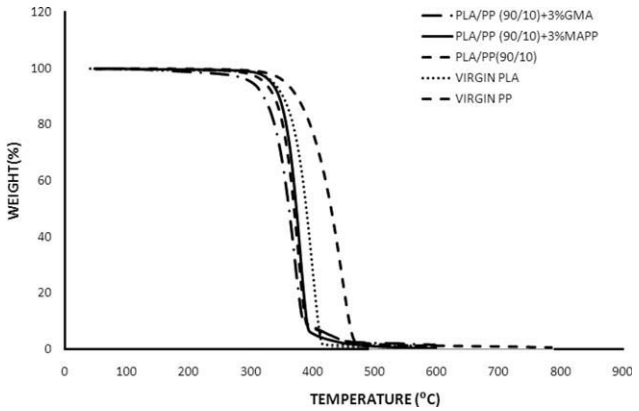

Figure 9 TGA curves for virgin PLA, PP, PLA/PP, PLA/PP/MAH-*g*-PP and PLA/PP/GMA.

the blend matrix due to the formation of bonds at the interface. The interaction of GMA with PLA also caused a slight increase in HDT compared with that of neat PLA.

CONCLUSIONS

Experimental findings revealed that PLA/PP blends at various ratios were successfully prepared with the melt-blending technique. Mechanical test results indicated an increase in the tensile modulus, tensile strength, flexural strength, and impact properties of PLA with the incorporation of PP. Further addition of MAH-*g*-PP increased TM, TS, FS, and IS by 6, 20, 47, and 17%, respectively. Thermal studies employing TGA revealed an increased thermal stability in the blend matrix. However, there was a decrease in the crystallinity and the presence of two distinct melting peaks, as observed from DSC thermograms. E' of PLA was found to increase in the blend matrix compatibilized with MAH-*g*-PP in comparison with that of the virgin PLA. The formation of interfacial bonds between PLA-MAH-*g*-PP and PP was also confirmed from the FTIR spectra. Furthermore, the morphological findings confirmed extensive plastic deformation with a homogenized dispersion of the PP phase within the PLA matrix in the presence of MAH-*g*-PP. Thus, on the basis of our observations, we concluded that PLA, being an inherently brittle polymer with limited thermal stability, was difficult to process. The incorporation of PP with a minimal concentration of 10 wt % led to improved processability. The PLA/PP blend constituted an immiscible system with a biphase morphology. The incorporation of suitable compatibilizers acted as a boundary between the two phases while improving the dispersion characteristics of the PP phase and enhancing the overall properties in the system.

References

1. Bastioli, C. Handbook of Biodegradable Polymers; Rapra Technology: Shropshire, England, 2005.
2. Aslan, S.; Calandrelli, L.; Laurienzo, P. J Mater Sci 2000, 35, 1615.
3. Kaplan, D. L.; Mayer, J. M.; Stenhouse, P. Fundamentals of Biodegradable Polymers; Technomic: Lancaster, PA, 1993; p 1.
4. Maiti, P.; Yamada, K.; Okamoto, M.; Ueda, K.; Okamoto, K. Chem Mater 2002, 14, 4654
5. Coltelli, M. B.; Maggiore, I. D. J Appl Polym Sci 2008, 110, 1250.
6. Noda, I.; Satkowski, M. M.; Dowrey, A. E.; Marcott, C. Macromol Biosci 2004, 4, 269.
7. Anderson, K. S.; Lim, S. H.; Hillmyer, M. A. J Appl Polym Sci 2003, 89, 3757.
8. Anderson, K. S.; Hillmyer, M. A. Polymer 2004, 45, 8809.
9. Girija, B. G.; Sailaja, R. R. N.; Madras. G. Polymer 2005, 90, 147.
10. Krause, S.; Goh, S. H. In. Polymer Handbook; Wiley: New York, 1999.
11. Li, Y. J.; Shimizu, H. Eur Polym J 2009, 45, 738.
12. Noda, I.; Satkowski, M. M.; Dowrey, A. E.; Marcott, C. Macromol Biosci 2004, 4, 269.
13. Anderson, K. S.; Lim, S. H.; Hillmyer, M. A. J Appl Polym Sci 2003, 89, 3757.
14. Lu, J. M.; Qiu, Z. B.; Yang, W. T. Polymer 2007, 48, 4196.
15. Zhang, C. L.; Feng, L. F.; Gu, X. P.; Hoppe, S.; Hu, G. H. Polymer 2007, 48, 5949.
16. Kim, J.; Zhou, H. Y.; Nguyen, S. T.; Torkelson, J. M. Polymer 2006, 47, 5799.
17. Dıaz, M. F.; Barbosa, S. E.; Capiati, N. J. Polymer 2007, 48, 1058.
18. Bhattacharyya, A. R.; Ghosh, A. K.; Misra, A. Polymer 2005, 46, 1661.
19. Guerrica-Echevarria, G.; Eguiazabal, J.; Nazabal, J. Eur Polym J 2007, 43, 1027.
20. Aro'stegui, A.; Naza'bal, J Polymer 2003, 44, 239.
21. Chapleau, N.; Huneault, M. A. J Appl Polym Sci 2003, 90, 2919.
22. Huang, J.; Paul, D. R. Polymer 2006, 47, 3505.
23. Shi, D.; Yang, J. H.; Yao, Z. H.; Wang, Y.; Huang, H. L.; Jing, W. Polymer 2001, 42, 5549.
24. Jiang, C. H.; Filippi, S.; Magagnini, P. Polymer 2003, 44, 2411.
25. Mohanty, S.; Nayak, S. K.; Verma, S. K.; Tripathy, S. S. J Reinf Plast Compos 2004, 23, 625.
26. Ton That, M. T.; Perrin Sarazin, F.; Cole, K. C.; Bureau, M. N.; Denault, J. Polym Eng Sci 2004, 44, 1212.
27. Manias, E.; Touny, A.; Wu, L.; Strawhecker, K.; Lu, B.; Chung, T. C. Chem Mater 2001, 12, 3516.
28. Zhai, H.; Xu, W.; Guo, H.; Zhou, Z.; Shen, S.; Song, Q. Eur Polym J 2004, 40, 2539.
29. Kim, Y. F.; Choi, C. N.; Kim, Y. D.; Lee, Y. K.; Lee, M. S. Fiber Polym 2004, 5, 270.
30. Wojciechowska, E.; Fabia, J.; Slusarczyk, C. Fiber Text East Eur 2005, 5(53), 126.
31. Ho, C. H.; Wang, C. H.; Lin, C. I.; Lee, Y. D. Polymer 2008, 49, 3902.
32. Mohanty, S.; Nayak, S. K. Int J Plast Tech 2008, 12, 1047.
33. Maiti, S. N.; Das, R. Int J Polym Mater 2005, 54, 467.
34. Gupta, A. K.; Purwar, S. N. J Appl Polym Sci 1985, 30, 1799.
35. Tomar, N.; Maiti, S. N. J Appl Polym Sci 2007, 104, 1807.
36. Handbook of Fillers and Reinforcements for Plastics; Katz, H. S.; Milewski, J. V., Eds.; Van Nostrand Reinhold: New York, 1987.
37. Piggot, M. R.; Leidner, J. J Appl Polym Sci 1974, 18, 1619.
38. Nicolais, L.; Narkis, M. Polym Eng Sci 1971, 11, 194.

39. Kunori, T.; Geil, P. H. J Macromol Sci Phys 1980, 18, 135.
40. Maiti, S. N.; Mahapatro, P. K. J Appl Polym Sci 1991, 42, 3101.
41. Guth, E.; Gold, O. Phys Rev 1938, 53, 322.
42. Aro'stegui, A.; Naza'bal, J. Polymer 2004, 44, 5227.
43. Jayanarayanan, K.; Joseph, K.; Thomas, S. Fiber Text East Eur 2005, 13(5), 122.
44. Chen, C. C.; Chueh, J. Y. Biomaterials 2003, 24, 1167.
45. Ravikumar, H. B.; Ranganathaiah, C. Polymer 2005, 46, 2372.
46. Aravind, I.; Albert, P.; Ranganathai, C. Polymer 2005, 45, 4925.
47. Mohanty, S.; Verma, S. K.; Nayak, S. K. Compos Sci Tech 2006, 66, 538.
48. Lewitus, D.; McCarthy, S.; Ophir, A.; Kenig, S. J Polym Environ 2006, 14, 171.
49. El Shafee, E.; Saad, G. R. J Polym Res 2008, 15, 47.
50. Kim, Y. F.; Choi, C. N. Fiber Polym 2004, 5, 270.